



Observation of Interplanetary Slow Shock Pair Associated with Reconnection Exhaust in Magnetic Cloud Boundary Layer

Zilu Zhou^{1,2} , Fengsi Wei^{1,3}, Xueshang Feng^{1,3} , Yi Wang³, Pingbing Zuo³ , and Xiaojun Xu⁴

¹ SIGMA Weather Group, State Key Laboratory for Space Weather, National Space Science Center, Chinese Academy of Sciences, Beijing 100190, People's Republic of China; zlzhou@swl.ac.cn

² University of Chinese Academy of Sciences, Beijing 100190, People's Republic of China

³ Laboratory for Space Weather Storms, Institute of Space Science and Applied Technology, Harbin Institute of Technology, Shenzhen 518000, People's Republic of China

⁴ Space Science Institute, Macau University of Science and Technology, Macao, People's Republic of China

Received 2018 April 17; accepted 2018 June 28; published 2018 August 13

Abstract

Magnetic reconnection is prevalent in the solar wind and is usually associated with interplanetary coronal mass ejections. We examined a Petschek-like reconnection exhaust (RE) in the front boundary of a magnetic cloud observed by the *WIND* spacecraft on 1998 June 2 and presented the first observation of a slow shock pair bounding the Petschek-like outflow jet in the interplanetary space. The whole structure contained an Alfvénic accelerated outflow and a pair of reverse slow shocks. The Alfvénic accelerated outflow was identified by Walén analysis. Rankine–Hugoniot relations were applied to confirm the slow shocks bounding the RE. Both shocks strictly satisfied the characteristics of slow shocks: (1) the intermediate Alfvén Mach numbers were both below unit in the up/downstream region; (2) the slow Mach number was above unit in the upstream side but below unit in the downstream side. Plasma was compressed and heated across the trailing slow shock, especially in the shock jump layer that has a temperature 2.4 times that of the upstream.

Key words: magnetic reconnection – shock waves – solar wind

1. Introduction

Magnetic reconnection is a fundamental process that converts magnetic energy into thermal and kinetic energy of plasma through merging and reconnecting of pairs of magnetic field lines. This process generally occurs at the thin current sheet with oppositely directed field lines and plays an important role in the space weather system.

Plenty of direct observations of magnetic reconnection at the magnetopause (e.g., Paschmann et al. 1979; Sonnerup et al. 1981) and magnetotail (e.g., Øieroset et al. 2000, 2001) have been reported in the last 50 years, but little attention was paid to this phenomenon in the solar wind until Gosling et al. (2005) presented direct evidence for magnetic reconnection in the solar wind based on the Petschek reconnection model (Petschek 1964). The key evidence for magnetic reconnection in solar wind reported by Gosling et al. (2005) was the Alfvénic accelerated or decelerated plasma jets in the field reversal regions. Using this identification, subsequent studies revealed that reconnection in the solar wind is commonly a large-scale and quasi-steady process (Davis et al. 2006; Phan et al. 2006; Gosling et al. 2007a), which is quite different from reconnection in the magnetopause and magnetotail. Reconnection is found to be prevalent in the low-speed and low proton β solar wind (Phan et al. 2009). Kinetic effects of collisionless reconnection have also been reported in the solar wind (Xu et al. 2015). A large number of reconnection events in the solar wind have been reported in association with interplanetary coronal mass ejections (iCMEs; e.g., Gosling et al. 2007b; Gosling & Szabo 2008; Xu et al. 2011), and it can at least occasionally be observed at the leading or trailing boundary of iCMEs (Gosling et al. 2007b; Wang et al. 2010; Ruffenach et al. 2012).

Magnetic clouds (MC), as a subset of iCMEs, are large-scale transient structures in the solar wind. MCs are characterized by

high magnetic field magnitude, the smooth rotation of the magnetic field direction, and low proton temperature (Burlaga et al. 1981). There is still no consistency among various approaches identifying MC boundaries, such as temperature decrease, density decrease, directional discontinuity, magnetic hole, bidirectional streaming of suprathermal electrons, and abrupt decrease in the intensity of low energy protons and plasma β . Wei et al. (2003a) suggested that the MC boundary is not a simple discontinuity but a complex boundary layer (BL) formed by the interaction between the MC main body and the ambient solar wind. The outer boundary of the BL, which separates the interaction region and the ambient solar wind, was characterized by the magnetic field intensity drop, the abrupt change of field direction, and the corresponding three-high state (i.e., relatively high proton temperature, density, and plasma β), while the inner boundary of the BL was identified by a three-low state, separating the interaction region and the MC main body. These characteristics in the MCBL are suggested to be manifestations of the magnetic reconnection process; thus, magnetic reconnection is supposed to play a common and important role in the formation of MCBL (Wei et al. 2003b, 2006). In addition, both physical modes and numerical simulations have demonstrated that reconnection could occur while the MC interact with the ambient solar wind (Dasso et al. 2006; Wang et al. 2010).

Slow shocks are a basic type of MHD shocks in the solar wind across which the magnetic field strength decreases from the upstream to the downstream. The plasma flow was sub-Alfvénic on both sides of a slow shock while the flow enters the shock at a speed larger than the upstream slow mode speed and leaves the shock at a speed less than the downstream slow mode speed. Unlike the large amount of other MHD discontinuities such as fast shocks, tangential discontinuities and rotational discontinuities, slow shocks have been seldom

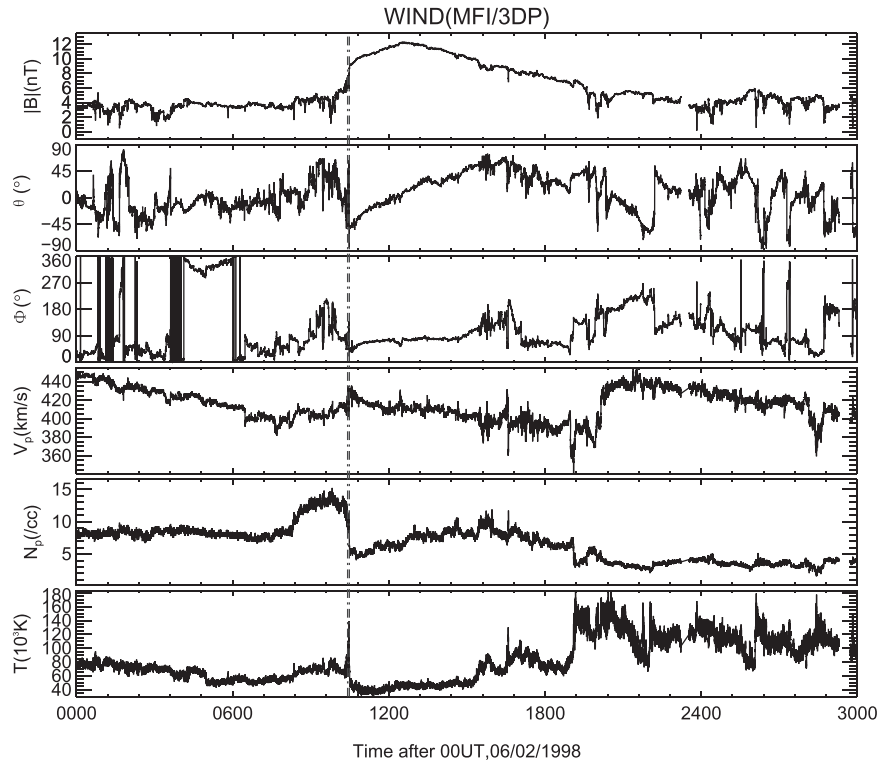


Figure 1. Magnetic cloud observed by *WIND* on 1998 June 2.

observed in interplanetary space (e.g., Chao & Olbert 1970; Burlaga & Chao 1971; Richter et al. 1985; Whang et al. 1996, 1998a, 1998b; Ho et al. 1998; Zuo et al. 2006; Zuo & Feng 2007). As observational evidence for Petschek-type reconnection, slow shocks bounding reconnection exhausts (REs) were also found in the magnetotail (e.g., Eriksson et al. 2004; Saito et al. 1995), but most reconnection events reported in the solar wind showed no evidence for the existence of such slow mode shocks (Gosling 2012). However, Zuo et al. (2006) identified a slow shock in MCBL and suggested that it probably was a signature of reconnection in the MCBL. Therefore, the relationship between slow shocks and the reconnection process in the MCBL is a very interesting topic.

In this paper, we report an RE bounded by two slow reverse shocks in an MCBL observed by *WIND* spacecraft on 1998 June 2. The Walén test is performed to identify the Alfvénic accelerated outflow jet (Section 2.2). We also perform the Rankine–Hugoniot equations to confirm the slow shock layers (Section 2.3). The results from this event study are discussed in Section 3, followed by a summary in Section 4.

2. Observations and Analyses

2.1. Observation of a Typical MCBL on 1998 June 2

Figure 1 shows an MC observed by the *WIND* spacecraft on 1998 June 2. The location of *WIND* was $(190.1, 3.5, 17.4)R_E$ in GSE. A typical front BL was identified during 10:25–10:29 UT, bounded by the dashed lines marked as M_f and G_f , as defined by Wei et al. (2003a). The front boundary of this MCBL (M_f) is associated with lower magnetic field strength B_t , higher proton temperature T_p , higher proton density N_p , and higher plasma β , while the inner boundary G_f is associated with higher B_t and lower T_p , N_p , plasma β .

Figure 2 presents more detailed magnetic field and plasma data in the MCBL using 3-s averaged data from *WIND* in the GSE coordinate system. The yellow shaded region near M_f is likely a bifurcated current sheet (hereafter, CS), inside which the magnetic field strength (Figures 2(a) and (f)) decreases with abrupt directional changes, while proton velocity (Figures 2(b) and (g)), proton number density (Figure 2(c)), and temperature (Figure 2(d)) have a strong enhancement. The blue shaded region in the rear of the CS (hereafter, SS1 layer) is a slow mode shock-like layer, across which the number density and temperature increase, while the magnetic field strength and proton velocity have a drop. The sum of plasma thermal pressure and magnetic pressure is displayed in Figure 2(e) and increases across the SS1 layer. The blue shaded region in the front of the CS (hereafter, SS2 layer) has a change similar to that of the SS1 layer. To give a strict confirmation of these substructures, we perform the Walén and Rankine–Hugoniot tests in the following sections, using the high resolution magnetic field data (92 ms) from MFI (Lepping et al. 1995) and plasma parameters (3 s) from 3DP (Lin et al. 1995) on the *WIND* spacecraft.

2.2. Analyses of the Alfvénic Accelerated Flow

To analyze the current sheet, we construct an LMN coordinate system. Here, the N component is the normal to the current sheet, the M -component is the X-line orientation, and the L -component is formed by the relation $\mathbf{M} \times \mathbf{N}$. We first calculate the normal to the current sheet (N) by performing a minimum variance analysis of the magnetic field (Sonnerup & Cahill 1967). We next use the relation $\mathbf{M} = \mathbf{N} \times (\mathbf{B}_A - \mathbf{B}_B)/|\mathbf{B}_A - \mathbf{B}_B|$ to determine the X-line orientation (M), where \mathbf{B}_A and \mathbf{B}_B are the tangential magnetic field vectors on the two sides of the current sheet (Sonnerup 1974). Then we calculate L using the relation $\mathbf{M} \times \mathbf{N}$.

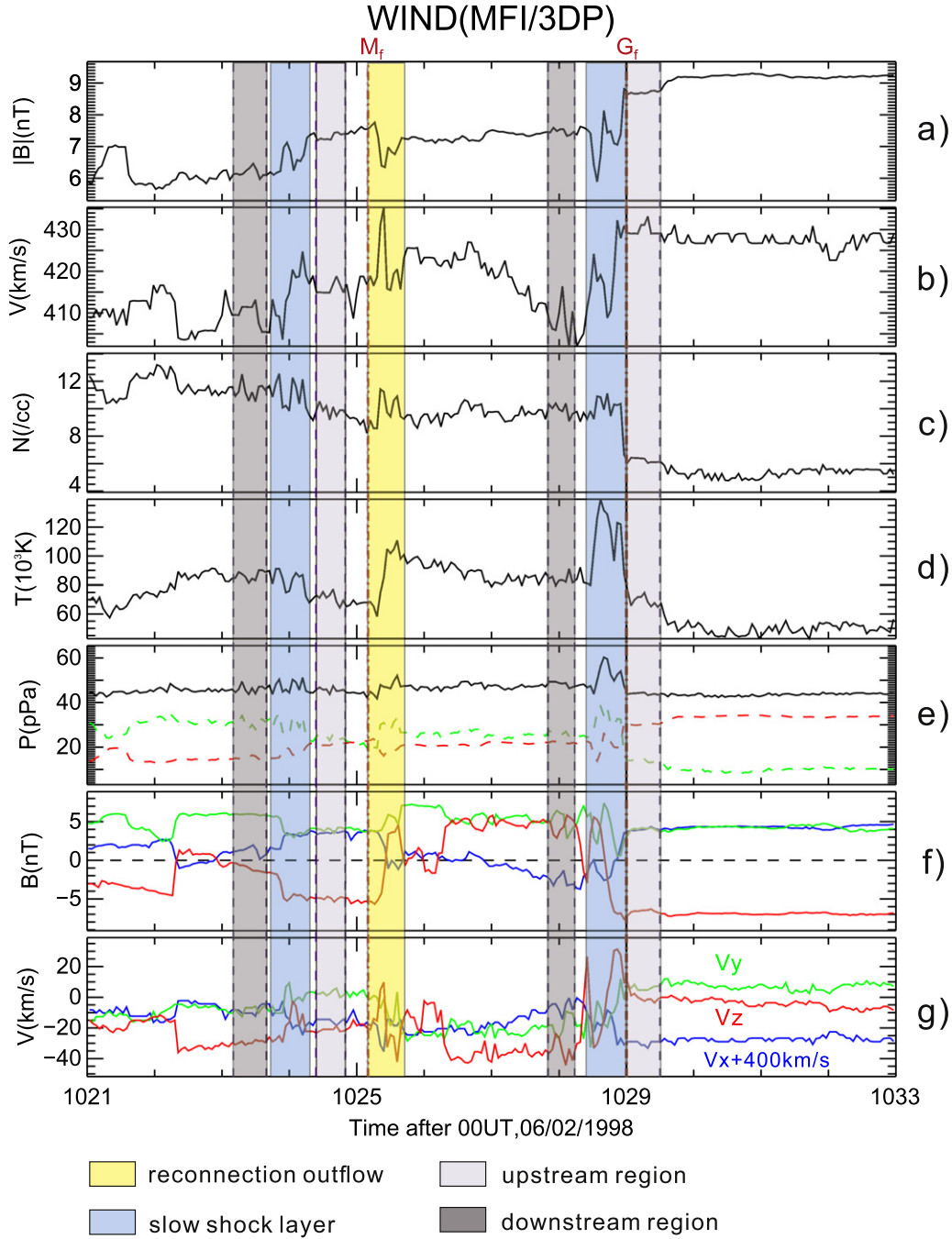


Figure 2. Magnetic field and plasma data in the MCBL: (a) magnetic field magnitude; (b) proton velocity; (c) proton number density; (d) proton temperature; (e) magnetic pressure (red), thermal pressure (green), and total pressure (black); (f) x, y, z components of magnetic field in GSE colored by blue, green, and red, respectively; (g) x, y, z components of proton velocity in GSE.

Furthermore, to identify the Alfvénic changes in the velocity components of the outflow jet, we perform the Walén test (Hudson 1970; Paschmann et al. 1986):

$$V_{\text{pre}} = V_{\text{ref}} \pm (1 - \alpha_{\text{ref}})^{(1/2)} (\mu_0 \rho_{\text{ref}})^{(-1/2)} [(\rho_{\text{ref}}/\rho) \mathbf{B} - \mathbf{B}_{\text{ref}}]. \quad (1)$$

Here, α is the pressure anisotropic factor and is defined as $\alpha \equiv (P_{\parallel} - P_{\perp})/\mu_0 |\mathbf{B}|^2$, where P_{\parallel} and P_{\perp} are the plasma pressures parallel and perpendicular to the magnetic field. In this paper, α is chosen to be zero due to the lack of such data. V , ρ , and \mathbf{B} denote the proton velocity, proton density, and

magnetic field. The subscript “ref” denotes the reference time at the leading or trailing edge of the reconnection outflow jet in the upstream region. The positive (negative) sign is chosen for the leading (trailing) edge of the jet.

We select the magnetic field data in the time period from 10:24 to 10:27 UT to calculate the normal to the current sheet. After performing the three steps introduced above, we obtain the normal direction \mathbf{n}_{cs} of (0.91, 0.31, 0.29) GSE. The X-line orientation obtained is (0.24, -0.94, 0.25) GSE and the L -direction is (-0.35, 0.16, 0.92). The shear angle of the magnetic field across the exhaust is 109° .

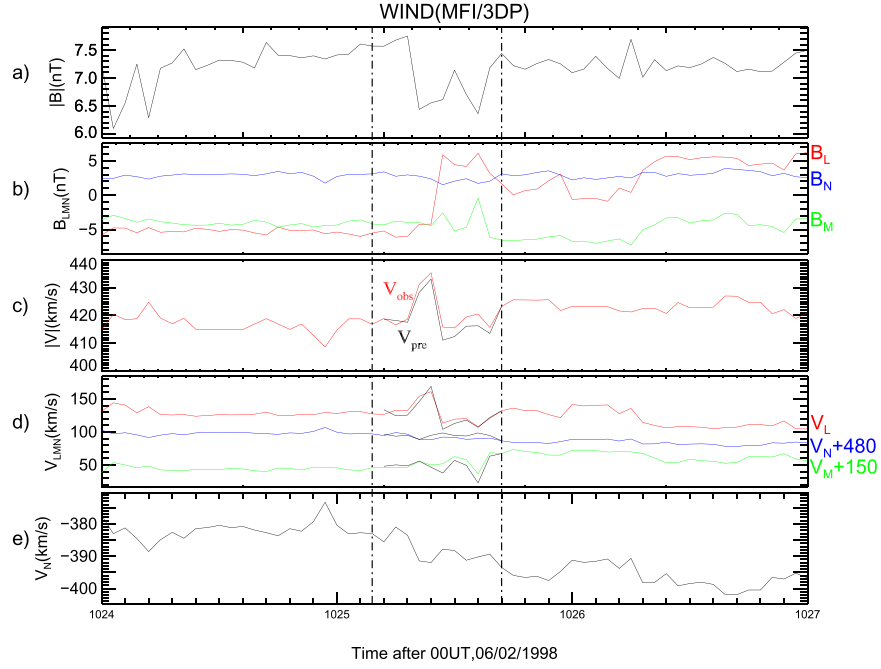


Figure 3. Walén test for the outflow. (a) Magnetic field magnitude; (b) magnetic field components in LMN coordinate system; (c) observed and predicted proton speed; (d) observed and predicted velocity components in LMN coordinate system; and (e) normal speed.

Figure 3 presents the magnetic field and proton velocity data in the LMN coordinate system. Figures 3(a), (c), and (d) show that the drop of magnetic field strength coincides with a strong enhancement in proton velocity. Figure 3(b) shows the L , M , N components of the magnetic field. B_N is nearly constant across the exhaust. B_L has a significant change from -5 to 5 nT. B_M is not zero, indicating the existence of an averaged 3 nT guide field in this RE.

Figure 3(c) shows the observed (red) and predicted (black) proton velocity magnitude of the jet. The predicted velocity from the Walén relation matches well with the observation. Figure 3(d) shows the observed and predicted velocity components in the LMN coordinate system. They match well in all three directions. Thus, the Walén test is satisfied for the accelerated outflow, which provides direct evidence for reconnection in the solar wind. The normal speed has a shift of 10 km s^{-1} across the exhaust, as shown in Figure 3(e). The mean Alfvén speed is about 50 km s^{-1} . Thus we simply estimate the reconnection rate V_{in}/V_A as $5/50 = 10\%$, which is in the range of fast reconnection.

2.3. Analyses of Slow Mode Shocks

The shock normal \mathbf{n} , pointing toward the upstream region with lower entropy, is a fundamental quantity of shocks. There are several methods for determining shock normal. Theoretically, using the coplanarity theorem (Colburn & Sonett 1966), the unit shock normal can be calculated as follows:

$$\mathbf{n} = \pm \frac{(\mathbf{B}_1 \times \mathbf{B}_2) \times (\mathbf{B}_2 - \mathbf{B}_1)}{|(\mathbf{B}_1 \times \mathbf{B}_2) \times (\mathbf{B}_2 - \mathbf{B}_1)|}. \quad (2)$$

Due to the existence of rotational discontinuities in REs, the magnetic field on both sides of a shock bounding the exhaust may no longer be coplanar. Thus the shock normal determined by the coplanarity theorem is not accurate enough for this case. Here we adopt a self-consistent method first introduced

by Zuo et al. (2006) to determine the shock normal, based on the Rankine–Hugoniot equations. Whang (1987) derived a set of formulae from Rankine–Hugoniot equations to calculate the downstream parameters using the given upstream conditions and shock normal. If θ and ϕ represent the latitude and azimuth angles of a unit vector, respectively, then we can use a parameter Δ to measure the averaged deviation of the observations from the predictions for arbitrary unit normal vector, which is defined as the function of θ and ϕ :

$$\Delta(\theta, \phi) = \sum \left(1 - \frac{X_{\text{pre}}}{X_{\text{obs}}} \right)^2, \quad (3)$$

where X_{pre} are the predicted postshock parameters calculated by the formulae proposed by Whang, that is, the number density N , the thermal pressure P , the sum of the proton temperature and electron temperature T , the magnitude of magnetic field B , the bulk velocity in the shock frame U_n , and X_{obs} are the measurements corresponding to X_{pre} . Hence, for each unit vector, the magnitude of Δ can be calculated. The shock normal is expected to coincide with the minimum Δ . In the present study, 180×360 unit vectors (180 for latitude angles and 360 for azimuth angles) are considered to search for the minimum Δ . The unit vector corresponding to the minimum Δ is convinced to be the shock normal. This self-consistent method will bring an uncertainty of $1^\circ \times 1^\circ$ in the $\theta - \phi$ parameter space, which is considered to be insignificant.

The two slow shock-like layers in this study are both suggested to be reverse shocks due to the anticorrelated changes in velocity and density, thus the shock speed is calculated by:

$$V_s = \frac{n_2 V_{n2} - n_1 V_{n1}}{n_2 - n_1} \quad (4)$$

Table 1
Selected Time Interval of Up/Downstream Region and Observed Flow Conditions (Averaged) of the “SS1” Layer

Parameters	Upstream	Downstream
Interval, UT	10:29:00–10:29:30	10:27:50–10:28:14
B_{gse} , nT	(3.99, 3.98, −6.61)	(−2.57, 5.02, 4.52)
V_{gse} , km s ^{−1}	(−430, 6.26, 0.24)	(−406, −17.5, −34.4)
N_i , /cc	6.25	9.95
T_i , 10 ³ K	66.3	83.8
T_e , 10 ³ K	91.1	107

in the inertial frame of reference and the normal bulk velocity of plasma in the shock frame of reference is obtained by:

$$U_n = V_n - V_s. \quad (5)$$

Here and in the following sections, V denotes the velocity in the inertial frame of reference and U denotes the velocity in the shock frame of reference. The subscript “ n ” denotes the components in the direction of shock normal. The up- and downstream parameters are denoted by the subscripts “1” and “2,” respectively.

2.3.1. Slow Shock Analysis for the Shock Layer Trailing the Jet

The fluctuations of magnetic field and proton velocity in the MCBL makes it difficult to select the time interval representative of the downstream region. We select a time interval of 24 s close to the SS1 layer that contains 261 data points for magnetic field and 8 for plasma parameters. The property of the shock remains the same after tuning the time interval slightly around. Thus we consider that the average values in the time interval we choose could represent the magnetic field and plasma conditions in the downstream region. The averaged up/downstream flow conditions are given in Table 1.

Then we adopt the self-consistent method introduced above to determine the shock normal. The normal direction \mathbf{n}_{ss1} is (0.84, 0.27, 0.47) in GSE. $B_{n1} = 1.335$ nT has a great agreement with $B_{n2} = 1.331$ nT. Meanwhile, the shock speed, the shock angle, and the bulk velocity in the shock frame are all calculated using the formulae in Whang’s paper. The results are given in Table 2. As introduced in Section 1, the bulk normal speed in the shock frame should satisfy these two conditions: (1) the intermediate Mach number $M_I = U_n/V_I = U_n/V_A \cos \theta_{Bn}$ is less than 1 on both sides of the shock; (2) the slow Mach number $M_s = U_n/C_s$ is larger than 1 in the preshock region and less than 1 in the postshock region, here C_s is the phase speed of the local slow magnetosonic wave. From Table 2, we can find that the intermediate Mach numbers are both below unit (0.70 in the preshock region and 0.55 in the postshock region), while the slow Mach number is 1.62 in the preshock region (>1) but is only 0.87 in the postshock region (<1). In addition, we compare the observed postshock conditions with the predicted postshock conditions calculated by the Rankine–Hugoniot equations, as shown in Table 3. The results reveal that the pre- and postshock conditions are in good agreement with the R–H relations. From these results, we recognize the “SS1 layer” as a slow shock with a compression ratio 1.60. Proton temperature in the shock jump layer is about 2.4 times that in the preshock region, indicating that plasma is significantly heated across the slow shocks, especially in the shock jump layer.

Table 2
The Shock Normal, Shock Speed, and Flow Conditions on Both Sides of the Reverse Slow Shock “SS1”

Parameters	SS1
\mathbf{n}_{ss1} , in GSE	(0.84, 0.27, 0.47)
V_{sh} , km s ^{−1}	−367
θ_{Bn1}	81°2
θ_{Bn2}	79°4
U_{n1} , km s ^{−1}	8.12
U_{n2} , km s ^{−1}	5.10
U_{n1}/V_{I1}	0.70
U_{n2}/V_{I2}	0.55
U_{n1}/C_{s1}	1.62
U_{n2}/C_{s2}	0.87

Table 3
Observations and Predictions from the R–H Relations of the Jump Conditions of the Slow Shock “SS1”

Parameters	Observations	R–H Solutions	Relative Error
B_2/B_1	0.86	0.78	9.3%
N_2/N_1	1.59	1.44	9.4%
$(T_i + T_e)_2/(T_i + T_e)_1$	1.21	1.30	6.9%
U_{n2}/U_{n1}	0.63	0.70	11.1%
P_2/P_1	1.93	1.87	3.1%

Table 4
Selected Time Interval of Up/Downstream Region and Observed Flow Conditions (Averaged) of the “SS2” Layer

Parameters	Upstream	Downstream
Interval, UT	10:24:24–10:24:50	10:23:10–10:23:40
B_{gse} , nT	(3.57, 4.01, −4.92)	(1.21, 5.95, −0.99)
V_{gse} , km s ^{−1}	(−415, 2.59, −21.3)	(−408, −8.01, −29.4)
N_i , /cc	9.9	11.3
T_i , 10 ³ K	68.2	107.8
T_e , 10 ³ K	86.4	111

2.3.2. Slow Shock Analysis for the Shock Layer Leading the Jet

The same method is applied to analyze the SS2 layer leading the jet. The averaged up/downstream flow conditions are given in Table 4.

The shock normal \mathbf{n}_{ss2} is found in the direction of (0.74, 0.65, 0.17) in GSE. $B_{n1} = 4.41$ nT has a good agreement with $B_{n2} = 4.57$ nT. The shock speed, the shock angle, and the bulk velocity in the shock frame are given in Table 5.

The intermediate Mach number are both below unit (0.82 in the preshock region and 0.74 in the postshock region), while the slow Mach number is 1.30 in the preshock region (>1) but is only 0.94 in the postshock region (<1). The R–H predictions are listed in Table 6. The pre- and postshock conditions are also in great agreement with the R–H relations. Therefore, the “SS2 layer” is also a slow shock. The compression ratio of this shock is only 1.15, which is relatively weak.

3. Results and Discussion

In the interplanetary space, a single spacecraft usually pass through exhausts on an alternative side of the reconnection sites, as pointed out in Gosling et al. (2005). When a spacecraft crosses such REs, a bifurcated current sheet would be observed. The Petschek model shows that the Alfvénic

Table 5

The Shock Normal, Shock Speed, and Flow Conditions on Both Sides of the Reverse Slow Shock “SS2”

Parameters	SS2
n_{s2} , in GSE	(0.74, 0.65, 0.17)
V_{sh} , km s ⁻¹	-336
θ_{Bn1}	52°8
θ_{Bn2}	42°0
U_{n1} , km s ⁻¹	25.2
U_{n2} , km s ⁻¹	21.9
U_{n1}/V_{I1}	0.82
U_{n2}/V_{I2}	0.74
U_{n1}/C_{s1}	1.30
U_{n2}/C_{s2}	0.94

Table 6

Observations and Predictions from the R–H Relations of the Jump Conditions of the Slow Shock “SS2”

Parameters	Observations	R–H Solutions	Relative Error
B_2/B_1	0.85	0.87	2.4%
N_2/N_1	1.15	1.16	0.9%
$(T_i + T_e)_2/(T_i + T_e)_1$	1.13	1.11	1.8%
U_{n2}/U_{n1}	0.87	0.86	1.1%
P_2/P_1	1.30	1.29	0.8%

accelerated outflow is bounded by a pair of slow shocks. In this study, *WIND* observed all the substructures indicated by the Petschek model. An ideal schematic of the exhaust is shown in Figure 4. *WIND* first passed through a slow shock layer (SS2) during 10:23:40–10:24:20 UT, then observed an Alfvénic accelerated outflow during 10:25:10–10:25:40 UT, which was trailing by a slow shock layer (SS1) during 10:28:20–10:29:00 UT, and finally encountered the MC main body. The Walén test was also implied (but not shown) on the region with a 2 minute interval between the outflow jet and SS1 layer. The results revealed that this region was filled with roughly Alfvénic fluctuations. Furthermore, the angle between the normal of the current sheet (n_{cs}) and “SS1” slow shock (n_{ss1}) is 11°3, coinciding with the bifurcated structure of localized current sheets. The angle between the shock normal and preshock magnetic field is 81°2, which classifies the SS1 shock into quasi-perpendicular shocks, which is also consistent with the Petschek model.

The angle between (n_{cs}) and (n_{ss2}) is 22°9, also coinciding with the bifurcated structure, but indicating asymmetry of the exhaust in this study. Indeed, for symmetric REs, the normal of either slow shock points to the direction of the inflow region. But in our case, the downstream region lies in the sheath region ahead of the MCBL. A possible cause is the asymmetric conditions on different sides of the exhaust. Magnetic reconnection occurs at the leading edge of the MC between plasmas with higher velocity but lower density and temperature in the MC and highly compressed and heated plasmas in the MCBL.

ACE encountered the MC with the shock layer at the leading edge about 7 minutes earlier at (224.4, 3.1, -21.6) R_E . The shock layers and outflow exhaust own a timescale of about 40 s, which is shorter than the time resolution of plasma data from *ACE*. Hence, we failed to get more information except for the transit time of this event from *ACE*. Feng et al. (2007) proposed the transit time could be used to distinguish slow

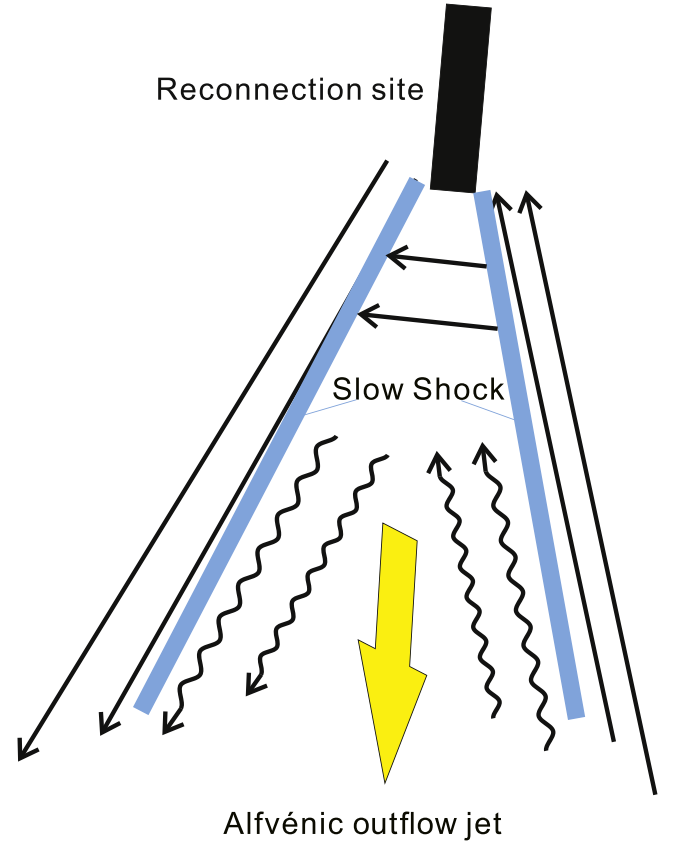


Figure 4. Idealized 2D schematic of Petschek-like exhausts. The wavy lines refer to rotational discontinuities and Alfvénic fluctuations of magnetic field lines.

shocks from tangential discontinuities. The transit time of planar discontinuities can be expressed as:

$$\Delta t = \Delta \mathbf{R} \cdot \mathbf{n} / V_d, \quad (6)$$

where $\Delta \mathbf{R}$ is the distance of the two spacecraft and V_d is the speed of discontinuity. Then we estimate that Δt is about 191 s, much less than the observational transit time. However, the number density and the plasma total temperature both have a significant enhancement from the upstream to downstream regions, especially in the shock jump layer. That is, the SS1 layer is obviously not a tangential discontinuity, across which the total pressure keeps balanced. Therefore, the discrepancy of the transit time is not caused by mistaking TDs for slow shocks. We suggest that the error in estimating the shock normal direction may partly account for the difference since the downstream region in the exhaust is filled with fluctuations. Another possible reason is the curvature of the shock surface.

Innocenti et al. (2015) found the Petschek-like Switch-Off Slow Shock/Rotational Discontinuity compound structure using a 2D kinetic simulation of collisionless magnetic reconnection. The exhaust was developed as a result of single X-point reconnection. In our case, an RD could also be identified during 10:26:05–10:26:30 UT, on the inner side of the SS1 layer. The direction of the magnetic field changed smoothly while the magnetic field magnitude, the number density, the proton/electron temperature, and the total pressure remained nearly unchanged. As mentioned above, the Walén relation was also satisfied, confirming this structure as an RD. Both slow shocks were not Switch-Off shocks, mainly because

the trajectory of *WIND* was far from the reconnection site. The consistency of the simulation results and the observation reveals that this compound structure observed in our study is probably formed by a single X-point reconnection in the MCBL.





4. Summary

In this study, we present a Petschek-like RE bounded by a slow shock pair in MCBL observed by *WIND* on 1998 June 2. Walén and Rankine–Hugoniot tests are applied to check the Alfvénic accelerated outflow and slow shock layers, respectively. The results of the Walén test reveal the bifurcated structure of the current sheet and the correlated (anticorrelated) changes in magnetic field and proton velocity. We use a self-consistent method to search the best-fit shock normals. The pre- and postshock intermediate Mach number and slow mode Mach number both satisfy the criteria of slow shocks. The good agreement between the observed and predicted postshock parameters indicates that the R–H relations are satisfied. The angle between the current sheet normal and shock normals also meet the bifurcated structure of the Petschek reconnection model.

Petschek REs in the solar wind have been intensively studied and are usually associated with iCMEs. But slow shocks bounding the exhausts are rarely identified in these previously reported cases. On the other hand, slow shocks in the MCBLs were recognized several years ago. Up to now, no direct evidence has revealed the relationship between the two phenomena in the MCBL. The results from our study present further evidence in favor of Petschek-like reconnection in the MCBLs. In turn, a Petschek-like reconnection process could be a source generating slow shocks in the MCBLs.

We thank the principal investigators of Wind 3DP and MFI and *ACE* SWEPAM and MAG experiments and CDAWeb for making the data used in this paper available. This work is jointly supported by the National Natural Science Foundation of China (41731067, 41531073, and 41504132) and the Specialized Research Fund for State Key Laboratories of China.

ORCID iDs

Zilu Zhou  <https://orcid.org/0000-0002-4463-8407>
 Xueshang Feng  <https://orcid.org/0000-0001-8605-2159>
 Pingbing Zuo  <https://orcid.org/0000-0003-4711-0306>
 Xiaojun Xu  <https://orcid.org/0000-0002-2309-0649>

References

- Burlaga, L., Sittler, E., Mariani, F., & Schwenn, R. 1981, *JGR*, **86**, 6673
 Burlaga, L. F., & Chao, J. K. 1971, *JGR*, **76**, 7516
 Chao, J. K., & Olbert, S. 1970, *JGR*, **75**, 6394
 Colburn, D. S., & Sonett, C. P. 1966, *SSRv*, **5**, 439
 Dasso, S., Mandrini, C. H., Démoulin, P., & Luoni, M. L. 2006, *A&A*, **455**, 349
 Davis, M. S., Phan, T. D., Gosling, J. T., & Skoug, R. M. 2006, *GeoRL*, **33**, L19102
 Eriksson, S., Øieroset, M., Baker, D. N., et al. 2004, *JGR*, **109**, A10212
 Feng, H. Q., Lin, C. C., Chao, J. K., et al. 2007, *JGR*, **112**, A10104
 Gosling, J. T. 2012, *SSRv*, **172**, 187
 Gosling, J. T., Eriksson, S., Blush, L. M., et al. 2007a, *GeoRL*, **34**, L20108
 Gosling, J. T., Eriksson, S., McComas, D. J., Phan, T. D., & Skoug, R. M. 2007b, *JGR*, **112**, A08106
 Gosling, J. T., Skoug, R. M., McComas, D. J., & Smith, C. W. 2005, *JGR*, **110**, A01107
 Gosling, J. T., & Szabo, A. 2008, *JGR*, **113**, A10103
 Ho, C. M., Tsurutani, B. T., Lin, R. P., et al. 1998, *GeoRL*, **25**, 2613
 Hudson, P. 1970, *P&SS*, **18**, 1611
 Innocenti, M. E., Goldman, M., Newman, D., Markidis, S., & Lapenta, G. 2015, *ApJL*, **810**, L19
 Lepping, R. P., Acuña, M. H., Burlaga, L. F., et al. 1995, *SSRv*, **71**, 207
 Lin, R. P., Anderson, K. A., Ashford, S., et al. 1995, *SSRv*, **71**, 125
 Øieroset, M., Phan, T. D., Fujimoto, M., Lin, R. P., & Lepping, R. P. 2001, *Natur*, **412**, 414
 Øieroset, M., Phan, T. D., Lin, R. P., & Sonnerup, B. U. 2000, *JGR*, **105**, 25247
 Paschmann, G., Papamastorakis, I., Baumjohann, W., et al. 1986, *JGR*, **91**, 11099
 Paschmann, G., Sonnerup, B. U. Ö., Papamastorakis, I., et al. 1979, *Natur*, **282**, 243
 Petschek, H. 1964, NASA SP-50, 425
 Phan, T. D., Gosling, J. T., & Davis, M. S. 2009, *GeoRL*, **36**, L09108
 Phan, T. D., Gosling, J. T., Davis, M. S., et al. 2006, *Natur*, **439**, 175
 Richter, A. K., Rosenbauer, H., Neubauer, F. M., & Ptityna, N. G. 1985, *JGR*, **90**, 7581
 Ruffenach, A., Lavraud, B., Owens, M. J., et al. 2012, *JGR*, **117**, A09101
 Saito, Y., Mukai, T., Terasawa, T., et al. 1995, *JGR*, **100**, 23567
 Sonnerup, B. U. 1974, *JGR*, **79**, 1546
 Sonnerup, B. U. Ö., & Cahill, L. J. 1967, *JGR*, **72**, 171
 Sonnerup, B. U. Ö., Paschmann, G., Papamastorakis, I., et al. 1981, *JGR*, **86**, 10049
 Wang, Y., Wei, F. S., Feng, X. S., et al. 2010, *PhRvL*, **105**, 195007
 Wei, F., Feng, X., Yang, F., & Zhong, D. 2006, *JGR*, **111**, A03102
 Wei, F., Liu, R., Fan, Q., & Feng, X. 2003a, *JGR*, **108**, 1263
 Wei, F., Liu, R., Feng, X., Zhong, D., & Yang, F. 2003b, *GeoRL*, **30**, 2283
 Whang, Y. C. 1987, *JGR*, **92**, 4349
 Whang, Y. C., Larson, D., Lin, R. P., Lepping, R. P., & Szabo, A. 1998a, *GeoRL*, **25**, 2625
 Whang, Y. C., Zhou, J., Lepping, R. P., & Ogilvie, K. W. 1996, *GeoRL*, **23**, 1239
 Whang, Y. C., Zhou, J., Lepping, R. P., et al. 1998b, *JGR*, **103**, 6513
 Xu, X., Wang, Y., Wei, F., et al. 2015, *NatSR*, **5**, 8080
 Xu, X., Wei, F., & Feng, X. 2011, *JGR*, **116**, A05105
 Zuo, P. B., & Feng, X. S. 2007, *SoPh*, **240**, 347
 Zuo, P. B., Wei, F. S., & Feng, X. S. 2006, *GeoRL*, **33**, L15107